THE IMPACT OF A STATIC-MIXING NOZZLE ON UNIFORMITY IN MATERIAL EXTRUSION LARGE-SCALE ADDITIVE MANUFACTURING

James C. Brackett[1], Elijah P. Charles[1], Tyler C. Smith[2], Ahmed A. Hassen[2], Vlastimil Kunc[2], Chad E. Duty[1,2]

[1]University of Tennessee – Knoxville
1512 Middle Drive
Knoxville, TN

[2]Manufacturing Demonstration Facility
Oak Ridge National Laboratory
2370 Cherahala Blvd
Knoxville, TN

ABSTRACT

There are many methods of incorporating more than one material in Additive Manufacturing (AM) processes. Oak Ridge National Laboratory has developed a unique solution that enables in-situ material switching by developing a dual-hopper feed system for Cincinnati's Big Area Additive Manufacturing (BAAM) system. Continuous extrusion during a step-change in material feedstock results in a unique blended material transition region that exhibits a heterogeneous internal morphology. To improve mixing of materials during extrusion, a customized static-mixing nozzle was created for use with the BAAM. Single-bead transitions from Material A to B and B to A were printed with the mixing nozzle at a specified screw speed. Compositional analysis tracked the progression of the material transition as a function of extrudate volume. The resulting transition curves were compared against a standard nozzle configuration. Optical microscopy of cross-sections also demonstrated that the static-mixing nozzle promoted a more uniform bead geometry as well as a more homogeneous internal structure throughout the material transition.

Keywords: Additive Manufacturing, Polymer Extrusion, Multiple Materials
Corresponding author: James Brackett, jbracke4@vols.utk.edu
DOI: (will be filled by SAMPE)

SAMPE Conference Proceedings. Charlotte, NA, May 23-26, 2022. Society for the Advancement of Material and Process Engineering – North America.

DOI: (Will be added by SAMPE)

1. INTRODUCTION

Commonly known as 3D printing, Additive Manufacturing (AM) has been one of the fastest growing fields with instruments capable of processing metals [1-3], ceramics[4], and polymers [5-8]. While each AM platform requires a particular material form, from photosensitive liquids to micron-sized powders, all AM techniques provide the ability to produce complex geometries that are difficult or impossible to manufacture with traditional methods [9, 10]. Polymer AM platforms can use thermoplastic or thermoset materials and are generally classified as Direct Write (DW) [11-14], Material Jetting (MJ) [15-17], , and Material Extrusion (ME) [7, 18-23].

1.1 Polymer Additive Manufacturing

Recent advancements in polymer AM have largely been driven by extruding fiber-reinforced composite materials[24]. As shown by Love et al, the inclusion of carbon fiber in thermoplastic extrusion is crucial for limiting the impacts of warping and residual stresses [19]. Additionally, carbon fiber and other compositing materials enable thermoplastic AM to compete with traditional thermoset manufacturing [25, 26]. While these advancements have been important steps in the development of AM techniques, a more recent area of focus has been Multi-Material (MM) construction. Seamless inclusion of MM in AM would allow for multi-purpose construction much better suited to end-use production.

1.2 Multi-Material Additive Manufacturing

MM construction offers an avenue to improve the performance of AM parts and expand applications for end use parts [27]. Some of the most common materials used in FFF for MM applications are ABS and Poly Lactic Acid (PLA). Brischetto et al. used a dual print head to print ABS-PLA sandwich structures and found decreased performance compared to a single-material PLA part. However, a PLA-PLA part made using two print heads closely resembled that of the ABS-PLA parts, indicating that deposition through separate nozzles may have caused excessive cooling, which reduced the strength of the interface [28]. Another study using ABS and PLA found that performance was linked to the number and location of material interfaces irrespective of the size of each material region, concluding that interfaces in the print direction were especially vulnerable to void formation and delamination failure [29]. Lopes et al. further demonstrated that the material boundary is both a physical (discrete interfaces) and chemical (polymer compatibility) issue using PLA, Polyethylene Terephthalate (PET), and Thermoplastic Polyurethan (TPU). Again, PLA-PLA parts produced using multiple nozzles were outperformed by a PLA part printed from a single source, which was attributed to discontinuities in the PLA-PLA parts created by switching nozzles. Furthermore, the study found a decrease in performance in PLA-PET and PLA-TPU parts compared to the PLA-PLA parts, highlighting the importance of chemical affinity in material interfaces [30].

There have also been extensive MM investigation using MJ platforms. Bartlett et al. designed a small-scale robot with excellent impact resistance by depositing a series of ten different photosensitive inks with slightly different rigidity. The final MM design demonstrated improved geometric accuracy and mechanical toughness compared to the single material designs [15]. Vu et al. also investigated MM parts using MJ, focusing on interfacial bonding and failure points. Although MM construction improved part performance, the interface between materials was the most common point of failure and fracture initiation [16, 17].

DOI: (Will be added by SAMPE)

1.3 Large-Format Additive Manufacturing

Large-Format Additive Manufacturing (LFAM) systems have recently seen significant interest and growth, especially with ME-based systems [31]. For example, the Big Area Additive Manufacturing (BAAM) system developed by Oak Ridge National Lab (ORNL) in conjunction with Cincinnati Incorporated [32] and the Large Scale Additive Manufacturing (LSAM) developed by Thermwood [33, 34] both implement screw-based extrusion systems on an FFF-style platform with great success. Not only do these systems offer some advantages compared to typical ME systems such as scale and rate of production, but they also have the ability to use pelletized feedstock as a source material, dramatically reducing cost while expanding material selection by eliminating the need for specialized feedstock preparation. ORNL-based investigations have capitalized on the flexibility this affords BAAM by installing a dual-hopper attachment to change pelletized feedstocks in-situ and utilize the extrusion screw to blend the material interface to maintain continuous deposition [35]. This dual-hopper approach to MM avoids the common pitfalls of discrete boundaries and the associated delamination and bonding issues by allowing the material interface to blur during extrusion, creating a continuous bi-material transition region.[36]. However, the dual-hopper process has unique features. Of primary interest is the blended transition region created by material mixing within the polymer melt during extrusion. While it successfully allows for in-situ transition from one material to another, the blended region typically exhibits a non-homogenous morphology within the printed bead. This morphology presented discrete regions of each material along with some regions where the two were mixed. Previous work demonstrated that this regional arrangement is likely to have significantly different mechanical properties in the different regions [37]. Although the BAAM is capable of switching extrusion screws based on the requirements of the materials, the geometry typically used to improve mixing has not shown enough of an impact to homogenously mix two distinct materials during a material transition. Cross-sectional analysis has shown that a regional arrangement remains when using the designated mixing screw [37]. As such, a static mixing nozzle was developed and implemented in the BAAM dual-hopper printing process to improve material mixing and achieve a more homogenous internal bead structure.

2. EXPERIMENTATION

This investigation utilized a standard set of BAAM parameters and dual-hopper attachment to analyze the effect of a static mixing nozzle on the material transition behavior and internal bead morphology. Transition behavior was assessed by comparing the component zones of a material transition printed with a standard nozzle to those of one printed with a mixing nozzle. To quantify the success of the mixing nozzle, cross-sectional analysis using optical microscopy compared samples from the blended region from each transition curve for changes in regional morphology.

2.1 BAAM Printing Parameters

Two materials provided by Techmer PM were used for all prints: HIFILL ABS 1512 3DP (ABS) and ELECTRAFIL ABS 1501 3DP (CF/ABS), a 20 wt % carbon fiber reinforced ABS. The pelletized feedstock was dried at 80° C for at least four hours before printing using the BAAM dual-hopper configuration. Thermal conditions were kept constant using a 250 ºC melt temperature, a 100 ºC bed temperature, and a 255 ºC nozzle temperature for each set of print

conditions. Each print was deposited onto ABS build sheets that were attached to the build platform. A custom static mixing nozzle utilizing internal barriers to periodically redirect flow with a 1.02 cm (0.40 in) diameter was used for all prints. Bead width and height were set to 1.40 cm (0.55 in) wide and 0.51 cm (0.20 in) tall. Due to the extended length and heating attachment required for the customized nozzle, the tamper typically included in BAAM prints was not used. The rotation speed of the extrusion screw was set to 300 rotations per minute (RPM), which requires a print head travel speed of 10.90 cm/s (4.29 in/s) to maintain chosen bead dimensions.

2.2 Print Geometry

A simple rectilinear serpentine geometry was chosen for each experimental set (Figure 1). Each print consisted of two continuous beads in a single layer that differed only in the transition direction. Starting at Point A in Figure 1, the dual-hopper switched from using ABS pellets to drawing from the CF/ABS pellet supply. The transition from depositing ABS to CF/ABS material occurred within the first continuous bead between Points A and B. At some position prior to Point B, the transition had completed and only CF/ABS was being deposited. At Point B, extrusion momentarily stopped for the extrusion head to move to Point C. At Point C, the dual-hopper switched from CF/ABS pellets to ABS pellets. Between Points C and D, the deposition material transitioned from CF/ABS back to ABS, which was completed well before Point D. At Point D, extrusion was again stopped, and the deposition nozzle moved back to Point A on the next layer. The long sides of the print geometry were 86.4 cm (34.0 in) while the short sections were 5.1 cm (2.0 in), giving a total length of 909.3 cm (358.0 in) between Points A and D.

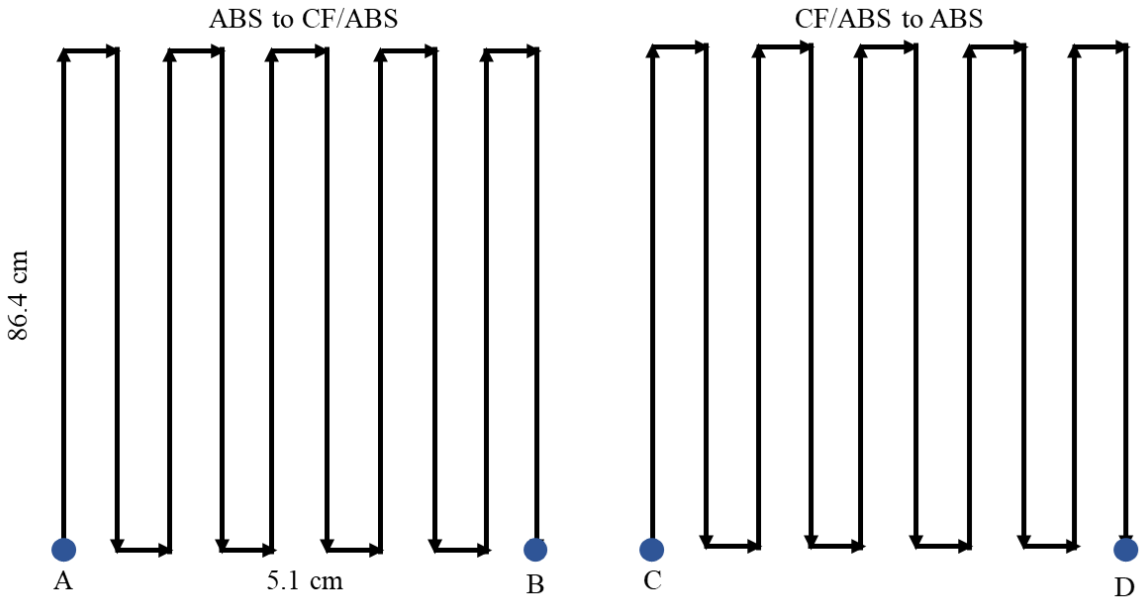

Figure 1. Schematic depiction of the deposition pattern for the printed material transitions.

2.3 Sample Extraction

Cross-sectional samples were extracted periodically from each print to develop a progression of the material composition. The position of a sample was determined by measuring the distance (L_S) from the point at which the hopper switch occurred (Points A and C in Figure 1) and converting

that to the extruded volume using Equation [1]. For simplicity, the cross-section was treated as rectangular with a thickness *t* and a width *w*. The nominal bead dimensions were expected to be 14.0 mm and 5.1 mm, giving a cross-sectional area of 71.4 mm^2. However, optical microscopy found the typical cross-sectional area to be best represented as 58.1 mm^2, which is investigated later. To better illustrate the degree of mixing that occurs during material switching, V_E was normalized by the free volume available in the extrusion system, V_F, as shown in Equation [2]. Due to the complex internal geometry of the extrusion system, the proprietary CAD model was used to find the free space that would already be occupied by Material A after a hopper switch to Material B. As a result, V_N, the normalized volume, represents "one transition's worth" of material when $V_N = 1$.

$$V_E = L_S \times t \times w \quad [1]$$

$$V_N = \frac{V_E}{V_F} \quad [2]$$

Printed transitions were initially sectioned into 7.6 cm (3.0 in) pieces and numbered sequentially to track position in the print. Individual samples for characterization were cut from the ends of these pieces using an Isomet 1000 diamond saw and were approximately 8.4 mm long. Previous work has proven an 8.4 mm sample to be a reliable representation of composition in the surrounding area [38]. Sample locations were initially chosen based on visual inspection of color change to estimate the beginning and ending of the transitions with intent to test more frequently within and around the transition zone. After initial characterization, additional samples were selected to fill in sparse areas on the transition curve and provide a comprehensive analysis of the transition from Material A to Material B.

2.4 Constituent Content Analysis

Samples were analyzed for carbon fiber content to determine the material composition. Ultrasonic Assisted Acid Digestion (UAAD) was used to separate the fibers from the thermoplastic matrix. Inspired by ASTM D3171-15 [39], UAAD was explored extensively and has proven to be an effective alternative to time-consuming carbonization-in-nitrogen and carbonization-in-air techniques [36, 40]. Before undergoing UAAD, samples were dried at 80 °C for at least four hours, then weighed using a RADWAG AS 220.R2 analytical balance to a 0.1 mg accuracy. Following UAAD, the solution was passed through glass microfiber filters with 1.5 µm pores to collect the separated fibers. After drying again at 80 °C for at least four hours, the fibers were again weighed and compared to the original mass of the specimen as shown in Equation [3]. *DR* was the Dissolution Ratio representing the expected fiber loss during UAAD and filtering found in [40], M_i was the dry mass of the printed specimen, M_c was the mass of pan and filter used to contain and collect the samples, and M_{cr} was the dried mass of pan and filter after fiber collection.

$$\text{Fiber wt \%} = \left(\frac{M_i - \left(\frac{M_i - (M_{cr} - M_c)}{1 - DR} \right)}{M_i} \right) = \frac{(M_{cr} - M_c) - M_i \times DR}{M_i \times (1 - DR)} \quad [3]$$

DOI: (Will be added by SAMPE)

2.5 Transition Curve Construction

Changes in material transition behavior when using the dual-hopper configuration were analyzed by comparing transition curves that plot against the normalized volume of material extruded since the hopper switch was initiated. As demonstrated in previous work [36, 40], the dual-hopper configuration produces three distinct stages of material transition during printing. Figure 2 shows these zones using an example transition curve The purge zone (orange) occurs immediately after switching material feedstock and is composed entirely of unmixed Material A that was already present in the barrel when the switch was made. The transition zone (yellow) describes the section of the print where material composition is continually changing due to blending of the material interface during the extrusion process. Finally, the steady-state zone (green) begins after material composition has stabilized and reached steady-state printing of Material B. Both the size of the zones and point-to-point variation of each transition curve are analyzed.

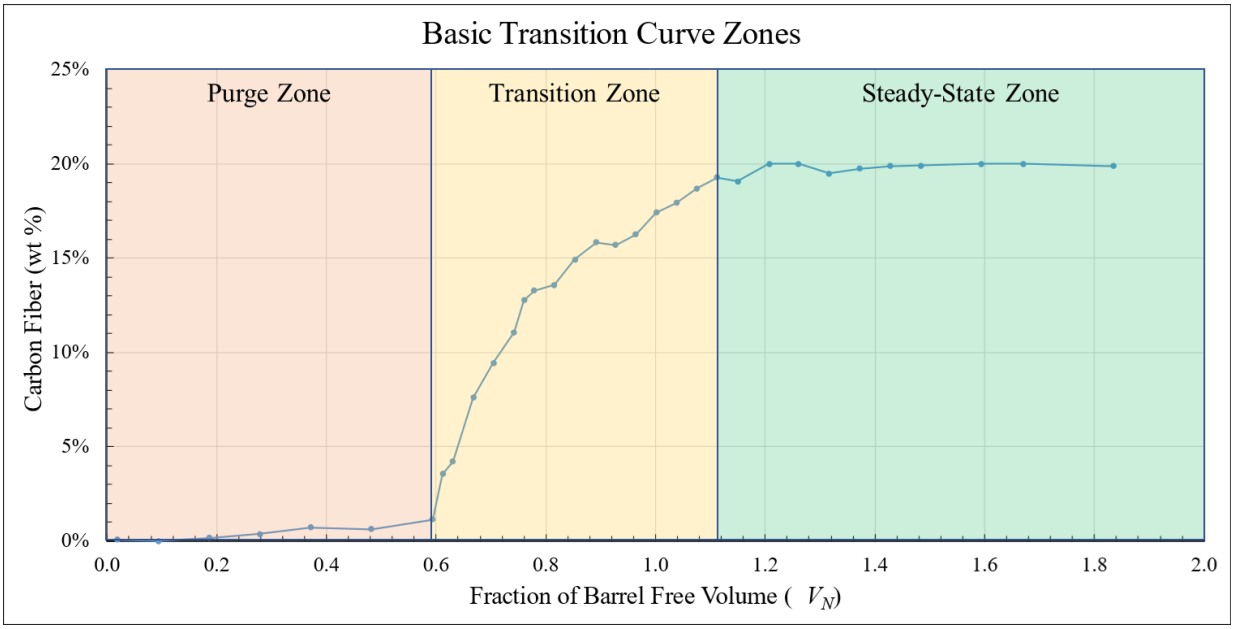

Figure 2. Example transition curve where the purge, transition, and steady-state zones are marked and represented by orange, yellow, and green, respectively.

2.6 Optical Microscopy

To investigate the impact of the mixing nozzle on the internal morphology of printed beads and judge the success of the design, optical images of sample cross-sections from before, within, and after the transition zone were taken. Before imaging, each specimen was polished using a six-slot AutoMet 250 autopolisher. The cross-sections were polished sequentially using 240, 320, 400, 600, and 800 SiC grit polishing pads for 1 minute each using 2 lb central force. The rotational speeds were set to 90 RPM for the platen and 60 RPM for the specimen holder in contrary rotational directions. A 1200 grit SiC paper was then used for 15 minutes with the same conditions. Finally, the polish was finished by using a 6 µm diamond suspension, a 3 µm diamond suspension, and colloidal silica for 20, 10, and 25 minutes respectively. These steps utilized a complementary rotation with both speeds set to 60 RPM. The sample surfaces were cleaned of debris using a

DOI: (Will be added by SAMPE)

sonicator filled with deionized water. Optical images were taken using a Keyonce VHX-5000 digital microscope and compared to cross-sections from prints that used a typical BAAM nozzle.

3. RESULTS

3.1 Impact of the Static Mixing Nozzle

Using the measured carbon fiber content, material composition was tracked as percent CF/ABS in both transition directions for all transition curves. Figure 3 shows a transition curve in each direction for a print using the static mixing nozzle and for another using a standard nozzle with otherwise identical settings. As stated previously, the purge zone ends and transition zone begins with a sudden change in material composition, but the end point of the transition zone and beginning of steady-state Material B can be difficult to identify, especially in the CF/ABS to ABS print direction. Per previous work, the CF/ABS feedstock can exhibit carbon fiber values as low as 19 wt % [40], so the steady-state zone for ABS to CF/ABS transitions was considered to begin where one data point and the following are both at or above 19 wt % carbon fiber. For the CF/ABS to ABS direction, steady-state Material B was determined on a case-by-case basis while considering the relative noise due to residual carbon fibers becoming stuck in the complex internal geometry. When comparing transition curves for the mixing nozzle to the standard nozzle in Figure 3, the ABS to CF/ABS direction demonstrated a slight delay in initiation of the transition zone and a longer transition zone overall. As would be expected, this led to a shorter overall transition to Material B for the standard nozzle. For the CF/ABS to ABS direction, the transition zone began earlier in the mixing nozzle, but a longer transition zone resulted in a near equal overall transition volume for both the CF/ABS to ABS transition curves.

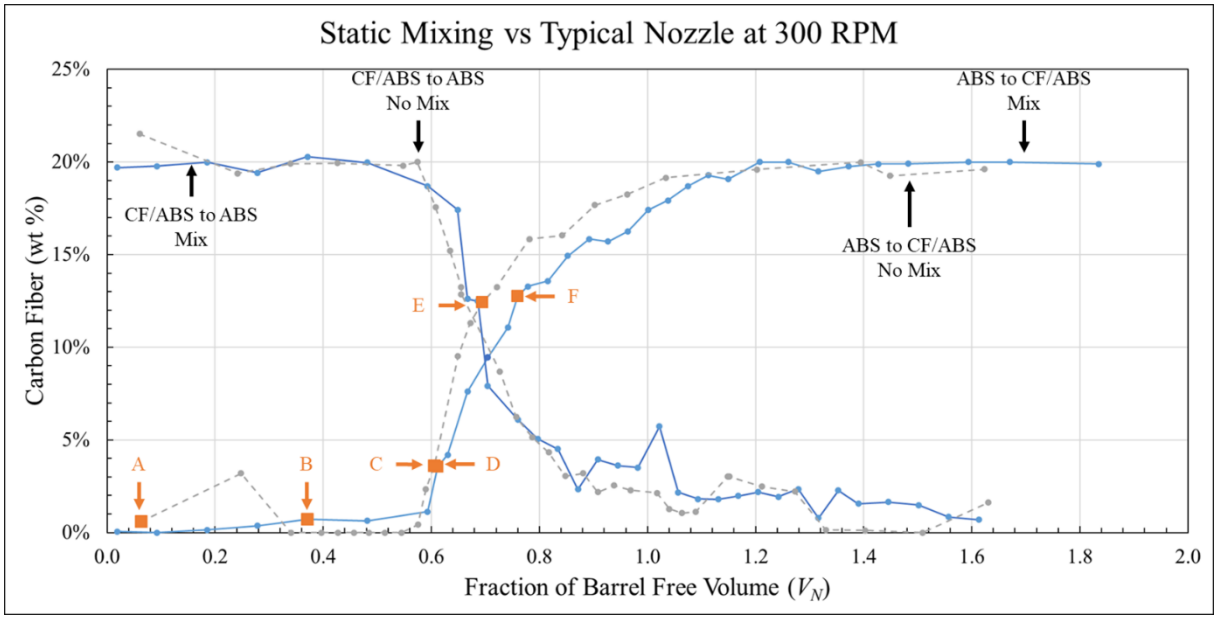

Figure 3. Transition curves at 300 RPM comparing the use of a mixing nozzle to that a standard nozzle. Six data points have been marked and labelled in orange for reference to Figure 4 in Section 3.2.

DOI: (Will be added by SAMPE)

3.2 Optical Imaging

The primary aim of introducing a static mixing nozzle was to improve the mixing of materials within the transition zone and eliminate discrete regions of Material A and B. Figure 4 shows cross-sections from the six orange, square data points labelled A through F in Figure 3 to match. The arrangement places standard nozzle samples on the top row and mixing nozzle samples on the bottom row with similar composition arranged vertically. Initial observations reveal a noticeable difference in bead shape between mixing and standard nozzle samples. Furthermore, there is a distinct difference in the morphology of the transition samples when comparing Figure 4C to 4D and Figure 4E to 4F. In both cases, the standard nozzle cross-sections exhibit a distinct regional morphology where there are clear pockets of both ABS and CF/ABS distributed throughout the bead. The mixing nozzle specimens do not display this regional behavior, indicating an increase in internal mixing that created a more homogenous internal bead structure, as desired. As shown, this was true at differing fiber contents and was consistent throughout the printed transitions, which aligned with the stated goal of improved material mixing when using the static mixing nozzle.

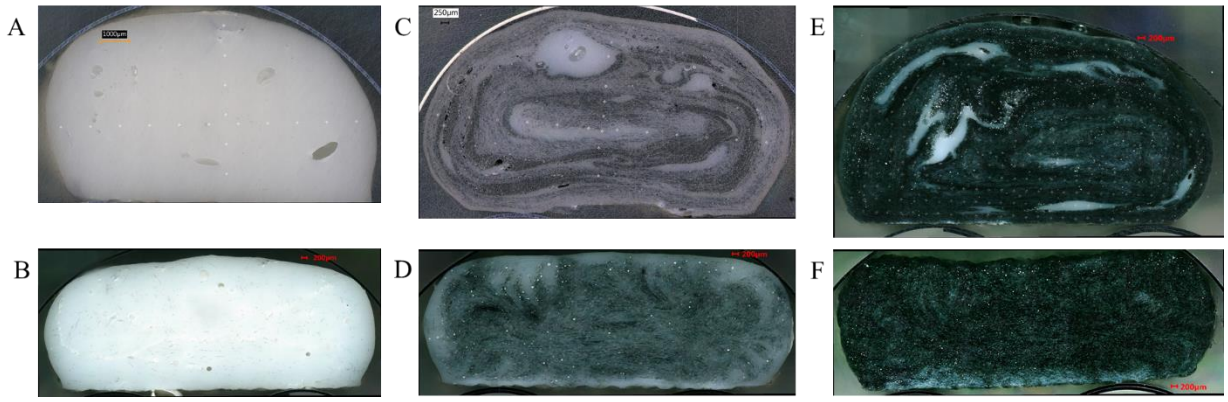

Figure 4. Optical cross sections taken at 200x of samples printed at 300 RPM with A), C), and E) printed using a typical nozzle while B), D), and F) were printed using the mixing nozzle. A) and B) were neat ABS, C) and D) were 3.6 wt % carbon fiber, E) and F) were 12. 4 wt % and 12.8 wt % carbon fiber respectively.

The improvements in homogeneity are highlighted in Figure 5, which compares the same location on the cross-sections in Figures 4E and 4F. Here, the standard nozzle sample in Figure 5A exhibits CF/ABS-rich, neat abs, and partially mixed regions all within this small section of the printed bead. In stark contrast, the mixing sample in Figure 5B maintains a consistent distribution of material throughout with only the bottom of the bead having any indication of a discrete neat ABS region. In addition, there is a distinctive pattern or swirl visible in the standard nozzle left as an artifact of the extrusion process that is not readily apparent in the mixing nozzle sample. As a result, mixing nozzle sample displays an much more homogenous morphology.

DOI: (Will be added by SAMPE)

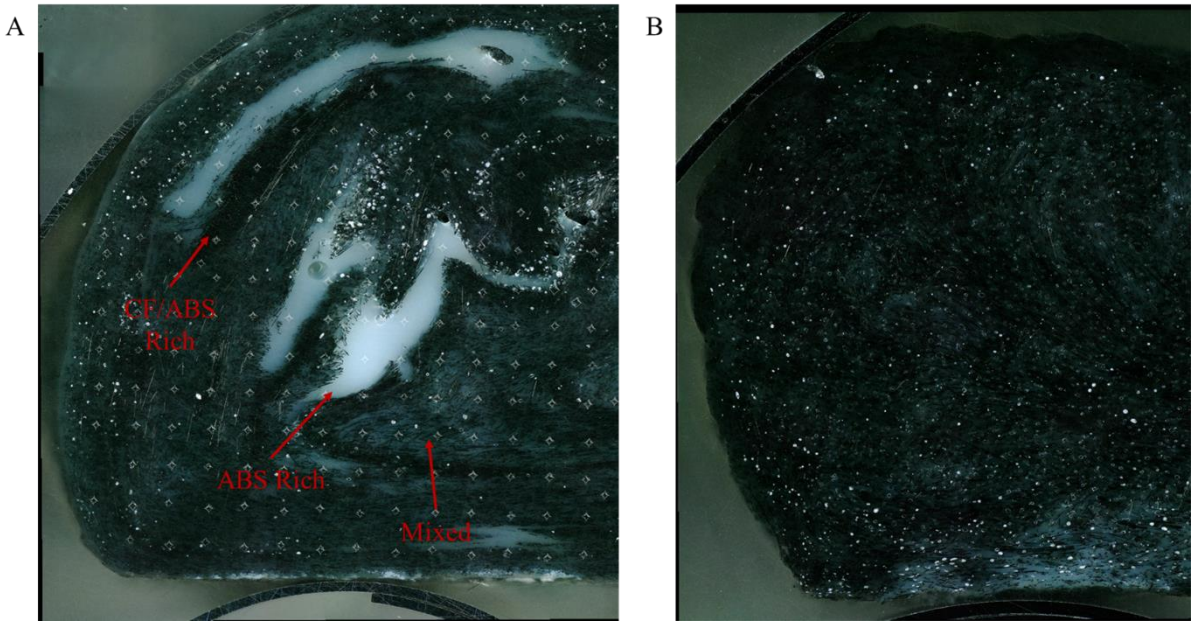

Figure 5. Expanded view of optical cross-sections from Figure 4A and 4C showing the extent of mixing differences. Marks on 5A are microhardness indentations for an analysis of mechanical properties that will follow this study.

3.2.1 Grayscale Analysis

To better quantify the improved mixing seen when using the mixing nozzle, the two cross sections shown in Figures 4E and 4F were analyzed using an image processor. After converting the images to an 8-bit grayscale image, a simple pixel count and distribution of values was recorded. The results are presented in Figure 6. The average grayscale value was 13.1 with a standard deviation of 14.6 for the mixing nozzle while the standard nozzle had an average grayscale value of 29.6 with a deviation of 25.6. As is seen in Figure 6, this shows a heavy, narrow weighting toward black for the mixing nozzle while there are many more instances of lighter counts causing a higher deviation for the standard nozzle. This results in a "tail" leading into the white values of the grayscale, which matches the visual observations of increased instances of ABS and unmixed material within the cross-sections.

DOI: (Will be added by SAMPE)

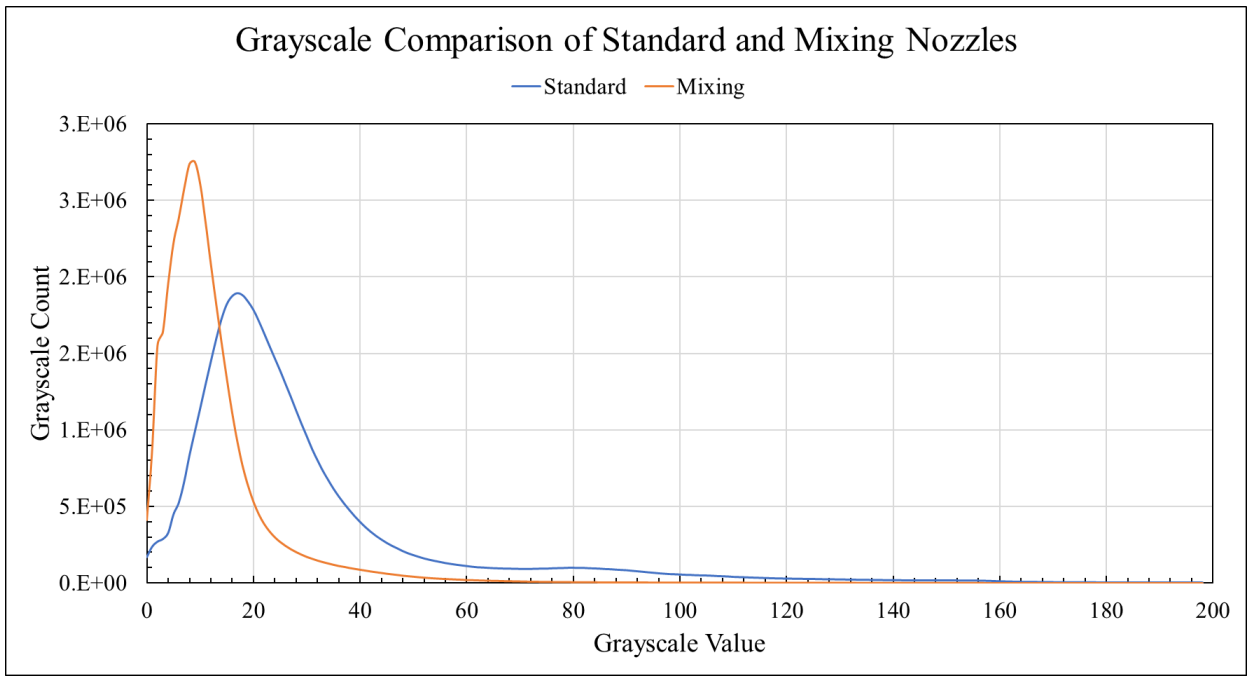

Figure 6. The Grayscale distribution of two samples with similar fiber content using the standard and mixing nozzle.

3.2.2 Bead Uniformity

In addition to improving mixing of the constituent materials, the mixing nozzle also impacted the uniformity and shape of the printed bead. Figure 7 compares the input dimensions provided to the BAAM (dashed, red rectangle) to both the standard (7A) and mixing (7B) nozzle cross-sections. As can be seen, the standard nozzle produces a much more elliptical bead than the mixing nozzle, which results in a near-rectangular cross-section well-suited to the volumetric treatments necessary for accurately calculating and forming the transition curves. Since the static mixing nozzle inhibits material flow with a complex internal geometry, an increase in back-pressure is to be expected. The increased back pressure would then counteract the drag flow, resulting in an overall decrease in material flow through the nozzle. In addition, the deposition rate remains constant. Therefore, the change in bead geometry and reduction in cross-sectional area matches expectations of a reduced flow deposited at the same rate as a with standard nozzle. This difference is highlighted in Section 2.3 when discussing the cross-sectional area utilized to calculate the normalized volume for the static mixing nozzle transition curves in Figure 3.

DOI: (Will be added by SAMPE)

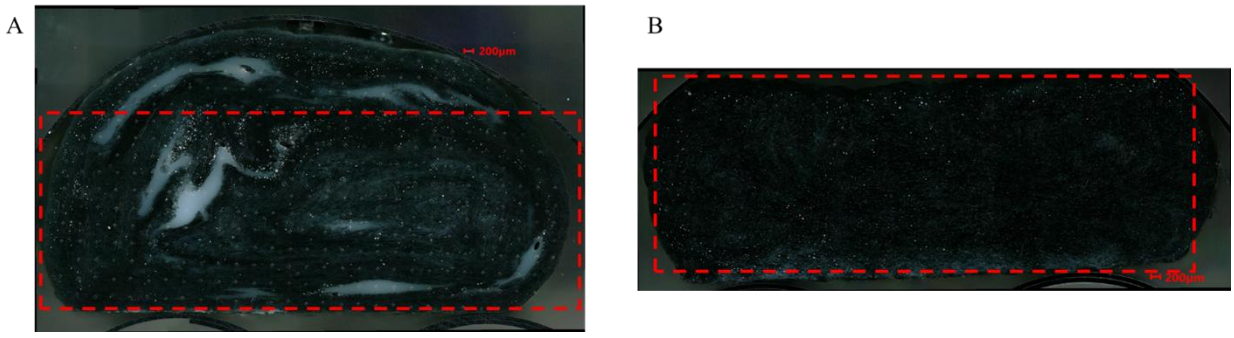

Figure 7. A.) A cross-section from a standard mixing nozzle and B.) a cross-section from the mixing nozzle transition print. The red, dashed rectangles represent the 14.0 mm by 5.1 mm bead dimensions input to BAAM.

3.2.3 Internal Porosity

While the inclusion of the static mixing nozzle improved mixing and dispersion of the component materials, there were also instances of porosity observed. As shown in Figure 8, optical imaging showed a significant amount of porosity in samples from both the purge and transition zones. However, Figure 8A exhibits larger pores with fewer instances whereas Figure 8B had a greater number of pores but with a smaller size. Further imaging indicated that pore size continued to decrease as fiber content increased.

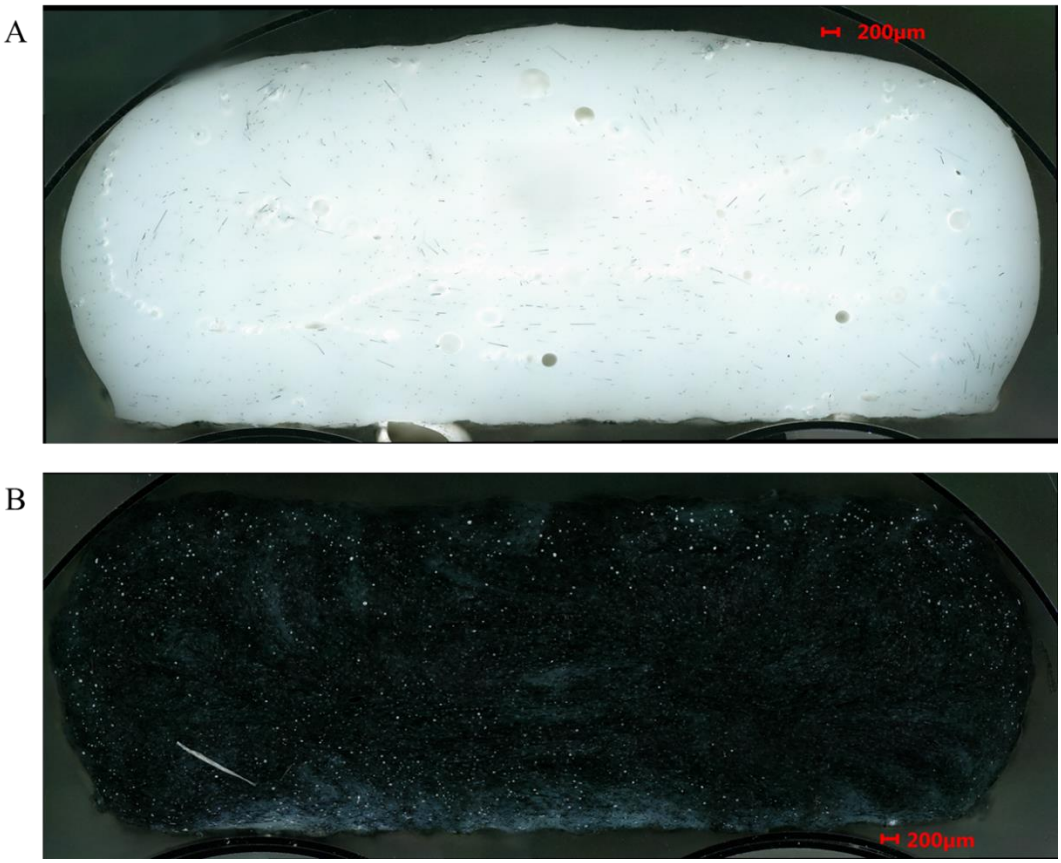

Figure 8. Optical images taken at 200x of polished cross-sections from the ABS to CF/ABS 300 RPM transition. A.) a Neat ABS specimen from the purge zone. B.) Transition Zone sample with 9.44 wt % carbon fiber.

DOI: (Will be added by SAMPE)

4. CONCLUSIONS

A static mixing nozzle was included in the BAAM dual-hopper material transition process to improve mixing of the constituent materials. The general transition behavior resembled that previously observed using a standard nozzle design with the mixing nozzle resulting in a slightly longer overall transition and increased instances of residual fibers. The recurring presence of carbon-fiber rich specimens indicates that the complex geometry of the mixing nozzle was retaining or trapping fibers that were later freed by the continuously flowing polymer melt. This effect was primarily seen in the CF/ABS to ABS transition direction, but a stair-stepping effect seen in the transition region of the ABS to CF/ABS transition curves could also be a possible artifact of the mixing nozzle. Optical microscopy demonstrated that the mixing nozzle successfully produced a more homogenous morphology than the standard nozzle design as desired. This was quantified by comparing grayscale distributions, which showed a significant weighting toward white (ABS) and higher deviation in the standard nozzle compared to the mixing nozzle.

Future investigations will focus on quantifying the degree of homogeneity observed in the cross sections via microhardness indentation. Following this, macroscopic effects will be assessed using mechanical characterization of full printed test specimens. Internal porosity will also be analyzed to determine if only the pore size changes with fiber content or if there is an influence on total porosity. Finally, additional compositional analysis will be conducted to clarify whether screw speed plays a defined role in transition behavior when printing with the mixing nozzle.

5. ACKNOWLEDGEMENTS

Research sponsored by the U.S. Department of Energy, Office of Energy Efficiency and Renewable Energy, Advanced Manufacturing Office, under contract DE-AC05-00OR22725 with UT-Battelle, LLC.

The authors would also like to acknowledge funding from the State of Tennessee and Tennessee Higher Education Commission (THEC) through their support of the Center for Materials Processing.

Further thanks to Cincinnati Incorporated and Techmer PM for provided Material and Equipment and the University of Tennessee – Knoxville Joint Institute for Advanced Materials's Metallography Lab group for collaboration.

6. REFERENCES

[1] Yan, J., Battiato, I., and Fadel, G. M. "A Mathematical Model-Based Optimization Method for Direct Metal Deposition of Multimaterials". *Journal of Manufacturing Science and Engineering* 139 (2017), DOI: 10.1115/1.4036424.

[2] Yan, J., Battiato, I., and Fadel, G. M. "Planning the process parameters for the direct metal deposition of functionally graded parts based on mathematical models". *Journal of Manufacturing Processes* 31 (2018): 56-71. DOI: https://doi.org/10.1016/j.jmapro.2017.11.001.

[3] Heinl, P., Muller, L., Korner, C., Singer, R. F., and Muller, F. A. "Cellular Ti-6Al-4V structures with interconnected macro porosity for bone implants fabricated by selective

electron beam melting". (in English), *Acta Biomaterialia* 4 (2008): 1536-1544. DOI: 10.1016/j.actbio.2008.03.013.

[4] Lakhdar, Y., Tuck, C., Binner, J., Terry, A., and Goodridge, R. "Additive manufacturing of advanced ceramic materials". *Progress in Materials Science* 116 (2021): 100736. DOI: https://doi.org/10.1016/j.pmatsci.2020.100736.

[5] Rodriguez-Panes, A., Claver, J., and Camacho, A. M. "The Influence of Manufacturing Parameters on the Mechanical Behaviour of PLA and ABS Pieces Manufactured by FDM: A Comparative Analysis". (in English), *Materials* 11 (2018): 21. Art no. 1333, DOI: 10.3390/ma11081333.

[6] Parandoush, P., Li, X., Chang, B., Sorensen, C. M., Shi, J., Liu, Y., and Lin, D. "Additive manufacturing of continuous carbon fiber reinforced epoxy composite with graphene enhanced interlayer bond toward ultra-high mechanical properties". *Polymer Composites* n/a (2021), DOI: https://doi.org/10.1002/pc.26423.

[7] Ning, F., Cong, W., Qiu, J., Wei, J., and Wang, S. "Additive manufacturing of carbon fiber reinforced thermoplastic composites using fused deposition modeling". *Composites Part B: Engineering* 80 (2015): 369-378. DOI: https://doi.org/10.1016/j.compositesb.2015.06.013.

[8] Wendel, B., Rietzel, D., Kuhnlein, F., Feulner, R., Hulder, G., and Schmachtenberg, E. "Additive Processing of Polymers". *Macromolecular Materials and Engineering* 293 (2008): 799-809.

[9] Attaran, M. "The rise of 3-D printing: The advantages of additive manufacturing over traditional manufacturing". (in English), *Business Horizons* 60 (2017): 677-688. DOI: 10.1016/j.bushor.2017.05.011.

[10] Berman, B. "3-D printing: The new industrial revolution". (in English), *Business Horizons* 55 (2012): 155-162. DOI: 10.1016/j.bushor.2011.11.003.

[11] Taylor, A. C., Beirne, S., Alici, G., and Wallace, G. G. "System and process development for coaxial extrusion in fused deposition modelling". *Rapid Prototyping Journal* 23 (2017): 543-550. DOI: doi:10.1108/RPJ-10-2015-0141.

[12] Kumar, P., Santosa, J. K., Beck, E., and Das, S. "Direct-write deposition of fine powders through miniature hopper-nozzles for multi-material solid freeform fabrication". (in English), *Rapid Prototyping Journal* 10 (2004): 14-23. DOI: 10.1108/13552540410512499.

[13] Compton, B. G. and Lewis, J. A. "3D-Printing of Lightweight Cellular Composites". *Advanced Materials* 26 (2014): 5930-5935. DOI: https://doi.org/10.1002/adma.201401804.

[14] Hmeidat, N. S., Elkins, D. S., Peter, H. R., Kumar, V., and Compton, B. G. "Processing and mechanical characterization of short carbon fiber-reinforced epoxy composites for material extrusion additive manufacturing". *Composites Part B: Engineering* 223 (2021): 109122. DOI: https://doi.org/10.1016/j.compositesb.2021.109122.

[15] Bartlett, N. W., Tolley, M. T., Overvelde, J. T. B., Weaver, J. C., Mosadegh, B., Bertoldi, K., Whitesides, G. M., and Wood, R. J. "A 3D-printed, functionally graded soft robot powered by combustion". (in English), *Science* 349 (2015): 161-165. DOI: 10.1126/science.aab0129.

[16] Vu, I., Bass, L., Meisel, N., Orler, B., Williams, C. B., and Dillard, D. A. "Characterization of Mutli-Material Interfaces in PolyJet Additive Manufacturing". *Solid Freeform*

Fabrication Symposium. Austin, TX, August, 2015. pp. 959-982. [Online]. Available: http://utw10945.utweb.utexas.edu/sites/default/files/2015/2015-79-Vu.pdf.

[17] Vu, I. Q., Bass, L. B., Williams, C. B., and Dillard, D. A. "Characterizing the effect of print orientation on interface integrity of multi-material jetting additive manufacturing". *Additive Manufacturing* 22 (2018): 447-461. DOI: https://doi.org/10.1016/j.addma.2018.05.036.

[18] Duty, C. E., Kunc, V., Compton, B., Post, B., Erdman, D., Smith, R., Lind, R., Lloyd, P., and Love, L. "Structure and mechanical behavior of Big Area Additive Manufacturing (BAAM) materials". *Rapid Prototyping Journal* 23 (2017): 181-189. DOI: doi:10.1108/RPJ-12-2015-0183.

[19] Love, L. J., Kunc, V., Rios, O., Duty, C. E., Elliott, A. M., Post, B. K., Smith, R. J., and Blue, C. A. "The importance of carbon fiber to polymer additive manufacturing". *Journal of Materials Research* 29 (2014): 1893-1898. DOI: 10.1557/jmr.2014.212.

[20] Tekinalp, H. L., Kunc, V., Velez-Garcia, G. M., Duty, C. E., Love, L. J., Naskar, A. K., Blue, C. A., and Ozcan, S. "Highly oriented carbon fiber-polymer composites via additive manufacturing". (in English), *Composites Science and Technology* 105 (2014): 144-150. DOI: 10.1016/j.compscitech.2014.10.009.

[21] Kotlinski, J. "Mechanical properties of commercial rapid prototyping materials". *Rapid Prototyping Journal* 20 (2014): 499-510. DOI: 10.1108/RPJ-06-2012-0052.

[22] Ning, F., Cong, W., Hu, Y., and Wang, H. "Additive manufacturing of carbon fiber-reinforced plastic composites using fused deposition modeling: Effects of process parameters on tensile properties". *Journal of Composite Materials* 51 (2017): 451-462. DOI: 10.1177/0021998316646169.

[23] Khondoker, M. and Sameoto, D. "Enhanced Bonding of Immiscible Polymers via Intermixed Co-extrusion in Fused Deposition Modelling". *41st Annual Meeting of the Adhesion Society*. San Diego, CA, February, 2018. [Online].

[24] Yuan, S., Li, S., Zhu, J., and Tang, Y. "Additive manufacturing of polymeric composites from material processing to structural design". *Composites Part B: Engineering* 219 (2021): 108903. DOI: https://doi.org/10.1016/j.compositesb.2021.108903.

[25] Nakagawa, Y., Mori, K.-i., and Maeno, T. "3D printing of carbon fibre-reinforced plastic parts". *The International Journal of Advanced Manufacturing Technology* 91 (2017): 2811-2817. DOI: 10.1007/s00170-016-9891-7.

[26] Yao, S.-S., Jin, F.-L., Rhee, K. Y., Hui, D., and Park, S.-J. "Recent advances in carbon-fiber-reinforced thermoplastic composites: A review". *Composites Part B: Engineering* 142 (2018): 241-250. DOI: https://doi.org/10.1016/j.compositesb.2017.12.007.

[27] Vaezi, M., Chianrabutra, S., Mellor, B., and Yang, S. "Multiple material additive manufacturing – Part 1: a review". *Virtual & Physical Prototyping* 8 (2013): 19-50. DOI: 10.1080/17452759.2013.778175.

[28] Brischetto, S., Ferro, C., Torre, R., and Maggiore, P. "3D FDM production and mechanical behavior of polymeric sandwich specimens embedding classical and honeycomb cores". *Curved and Layered Structures* 5 (2018): 80-94. DOI: 10.1515/cls-2018-0007.

[29] Kim, H., Park, E., Kim, S., Park, B., Kim, N., and Lee, S. "Experimental Study on Mechanical Properties of Single- and Dual-material 3D Printed Products". *Procedia Manufacturing* 10 (2017): 887-897. DOI: https://doi.org/10.1016/j.promfg.2017.07.076.

[30] Lopes, L. R., Silva, A. F., and Carneiro, O. S. "Multi-material 3D printing: The relevance of materials affinity on the boundary interface performance". *Additive Manufacturing* 23 (2018): 45-52. DOI: https://doi.org/10.1016/j.addma.2018.06.027.

[31] Kishore, V. and Hassen, A. A., "Chapter 6 - Polymer and composites additive manufacturing: material extrusion processes," in *Additive Manufacturing*, J. Pou, A. Riveiro, and J. P. Davim Eds.: Elsevier, 2021, pp. 183-216.

[32] Duty, C. E. and Love, L. J., "Cincinnati Big Area Additive Manufacturing (BAAM)," United States, 2015-03-04 2015. [Online]. Available: https://www.osti.gov/biblio/1210140 https://www.osti.gov/servlets/purl/1210140

[33] "LSAM - Large Scale Additive Manufacturing." http://www.thermwood.com/lsam_home.htm#whatislsam (accessed September 9, 2021).

[34] Wang, F., Ju, F., Rowe, K., and Hofmann, N. "Real-time control for large scale additive manufacturing using thermal images". *2019 IEEE 15th International Conference on Automation Science and Engineering (CASE)*. 22-26 Aug. 2019, 2019. pp. 36-41, doi: 10.1109/COASE.2019.8843264.

[35] Smith, T., Hassen, A. A., Lind, R., Lindahl, J., Chesser, P., Roschli, A., Kumar, V., Kishore, V., Post, B., Failla, J., Duty, C., Love, L., and Kunc, V. "Dual Material System for Polymer Large Scale Additive Manufacturing". *Society for the Advancement of Material and Process Engineering 2020*. Seattle, WA, May 4-7, 2020. [Online].

[36] Brackett, J., Yan, Y., Cauthen, D., Kishore, V., Lindahl, J., Smith, T., Sudbury, Z., Ning, H., Kunc, V., and Duty, C. "Characterizing material transitions in large-scale Additive Manufacturing". *Additive Manufacturing* 38 (2021): 101750. DOI: https://doi.org/10.1016/j.addma.2020.101750.

[37] Brackett, J., Charles, E., Cauthen, D., Smith, T., Kishore, V., Kunc, V., and Duty Chad, E. "The Impact of Processing Parameters on the Transition Behavior of Blended Material Large Scale 3D Printing". *Solid Freeform Fabrication Symposium*. Virtual, 12/1/2021, 2021. pp. 761-770.

[38] Brackett, J., Yan, Y., Cauthen, D., Kishore, V., Lindahl, J., Smith, T., Ning, H., Kunc, V., and Duty, C. "Development of Functionally Graded Material Capabilities in Large-scale Extrusion Deposition Additive Manufacturing". *Solid Freeform Fabrication Symposium*. Austin, TX, 2019. pp. 1793-1803. [Online]. Available: http://utw10945.utweb.utexas.edu/sites/default/files/2019/149%20Development%20of%20Functionally%20Graded%20Material%20Capabi.pdf.

[39] ASTM Standard D3171-15 2015, "Standard Test Methods for Constituent Content of Composite Materials" ASTM International, West Conshohocken, PA, 2015, DOI: 10.1520/D3171-15, https://www.astm.org/d3171-15.html.

[40] Brackett, J., Cauthen, D., Smith, T., Kunc, V., and Duty, C. "The Influence of Processing Parameters on the Transition Zone for Blended Material 3D Printing". *SAMPE 2020 Virtual Series | Additive Manufacturing*. Seattle, WA, June 1, 2020. [Online].